frontiers | Frontiers in Nanotechnology

TYPE Original Research
PUBLISHED 14 April 2025
DOI 10.3389/fnano.2025.1512622

OPEN ACCESS

EDITED BY
Long Binh Vong,
Vietnam National University, Vietnam

REVIEWED BY
Amit K. Roy,
Northeastern University, United States
Shivani R. Pandya,
Narnarayan Shastri Institute of Technology, India
Enyi YE,
Institute of Materials Research and Engineering (A*STAR), Singapore

*CORRESPONDENCE
Elena Alexander,
ei2169@columbia.edu

RECEIVED 17 October 2024
ACCEPTED 28 March 2025
PUBLISHED 14 April 2025

CITATION
Alexander E and Leong KW (2025) Toxicity and biodistribution comparison of functionalized nanodiamonds, quantum dot nanocarbons and gold nanoparticles.
Front. Nanotechnol. 7:1512622.
doi: 10.3389/fnano.2025.1512622

Toxicity and biodistribution comparison of functionalized nanodiamonds, quantum dot nanocarbons and gold nanoparticles

Elena Alexander* and Kam W. Leong

Department of Biomedical Engineering, Columbia University, New York City, NY, United States

Introduction: Nanomaterials are extensively utilized in applications ranging from electronics to biomedical therapies; however, their widespread use has prompted concerns about potential toxicity in humans. Understanding the biodistribution and toxicity profiles of nanoparticles is crucial for their safe application.

Methods: This study assessed the dose-dependent toxicity and biodistribution of unconjugated nanodiamonds, nanobody-conjugated nanodiamonds, gold nanoparticles, and quantum dot nanocarbons in 22 female C57BL/6 mice. Nanoparticles were intravenously administered at concentrations of 5, 10, 20, and 40 mg/kg. Samples were collected at 2, 24, and 96 hours post-administration to evaluate tolerability, immune responses, and biodistribution patterns.

Results: Unconjugated nanodiamonds showed favorable tolerability, eliciting minimal inflammatory responses and significantly lower memory T cell activation compared to gold nanoparticles and quantum dot nanocarbons. Nanobody-conjugated nanodiamonds triggered moderate inflammation at 2 hours post-dosing. Specifically, CD69 expression in $CD8^+$ T cells was highest in the gold nanoparticle group (mean: 0.40 $\pm$ 0.16) and lowest in the unconjugated nanodiamond group (mean: 0.12 $\pm$ 0.09). CD25 expression was most elevated in quantum dot nanocarbons (mean: 0.23 $\pm$ 0.04) and lowest in nanobody-conjugated nanodiamonds (mean: 0.09 $\pm$ 0.04). Total T cells were highest in the nanobody-conjugated group (mean: 49.10% $\pm$ 6.99) and lowest in the unconjugated nanodiamond group (mean: 40.70% $\pm$ 8.10). Nanodiamonds primarily accumulated in the heart, whereas gold nanoparticles localized mainly in the left lung, and quantum dot nanocarbons predominantly persisted in the kidney, liver, blood, and heart.

Discussion: These results indicate that nanodiamonds exhibit favorable tolerability and controlled immune responses compared to gold nanoparticles and quantum dot nanocarbons, highlighting their potential as safer nanomaterials for biomedical applications.

KEYWORDS

nanodiamonds, biodistribution, toxicity, nanoparticles, nanocarbons

1 Introduction

Nanoscience and nanotechnology are rapidly advancing fields, driving interest in submicron materials. Carbon nanomaterials, such as fullerenes, nanotubes, graphene, and nanodiamonds (NDs), are increasingly being utilized in materials science and nanotechnology industries for applications such as drug delivery, disease diagnosis, and treatment (Sun et al., 2002; Williams et al., 2002; Liu et al., 2008; Huang et al., 2007). However, their widespread use raises concerns about potential human exposure and associated toxicological effects (Vega-Villa et al., 2008; Aillon et al., 2009a). Therefore, the present study aimed to evaluate the toxicity and biodistribution of NDs (Figure 1). To provide a comprehensive analysis, we also compared the results with quantum dot nanocarbons, which belong to the same carbon nanoparticle family as NDs and are favored for their small size and excellent biocompatibility, as well as with gold nanoparticles, which are among the most well-studied and widely used nanoparticles in the industry (Molaei, 2019; Hammami et al., 2021).

1.1 Nanodiamonds and immunogenicity

NDs have been investigated for their potential to improve human health by modulating the immune system. Functionalizing the ND surface with antibodies or small molecules can elicit specific immune responses, such as increased proliferation of T cells, B cells, neutrophils, and macrophages (Paladhi et al., 2022; Chang et al., 2003; Pentecost et al., 2019; Huang et al., 2017; Suarez-Kelly et al., 2017; Ghoneum et al., 2010). Other applications focus on minimizing or eliminating immune responses to particles, such as using functionalized NDs to accumulate around damaged tissues for stem-cell repair or injecting fluorescent NDs for bioimaging (Liu et al., 2021; Alexander et al., 2019; Ansari et al., 2016; Lin et al., 2023; van der Laan et al., 2020).

Differences in nanomaterials make it challenging to generalize potential toxicological effects. Factors such as size, shape, concentration, exposure duration, and administration method influence the toxicity and biodistribution of nanomaterials (Aillon et al., 2009a; Xu et al., 2007; Muller et al., 2005; Yuan et al., 2009; Puzyr et al., 2007). The toxicity of NDs has been evaluated in several *in vitro* studies, but the results remain inconclusive. While many studies report NDs to be the least toxic carbon nanomaterial, others have observed concentration-dependent toxicities (Villalba et al., 2012). Gold nanoparticles are also a popular alternative to nanocarbons and are widely used in protein delivery, imaging, and cancer treatments. However, factors like size, surface charge, and shape play crucial roles in determining their uptake, biodistribution, and toxicity. For instance, nanoclusters of 1.4 nm have shown increased toxicity in various cell lines compared to clusters of 0.8, 1.2, and 1.8 nm (Aillon et al., 2009a).

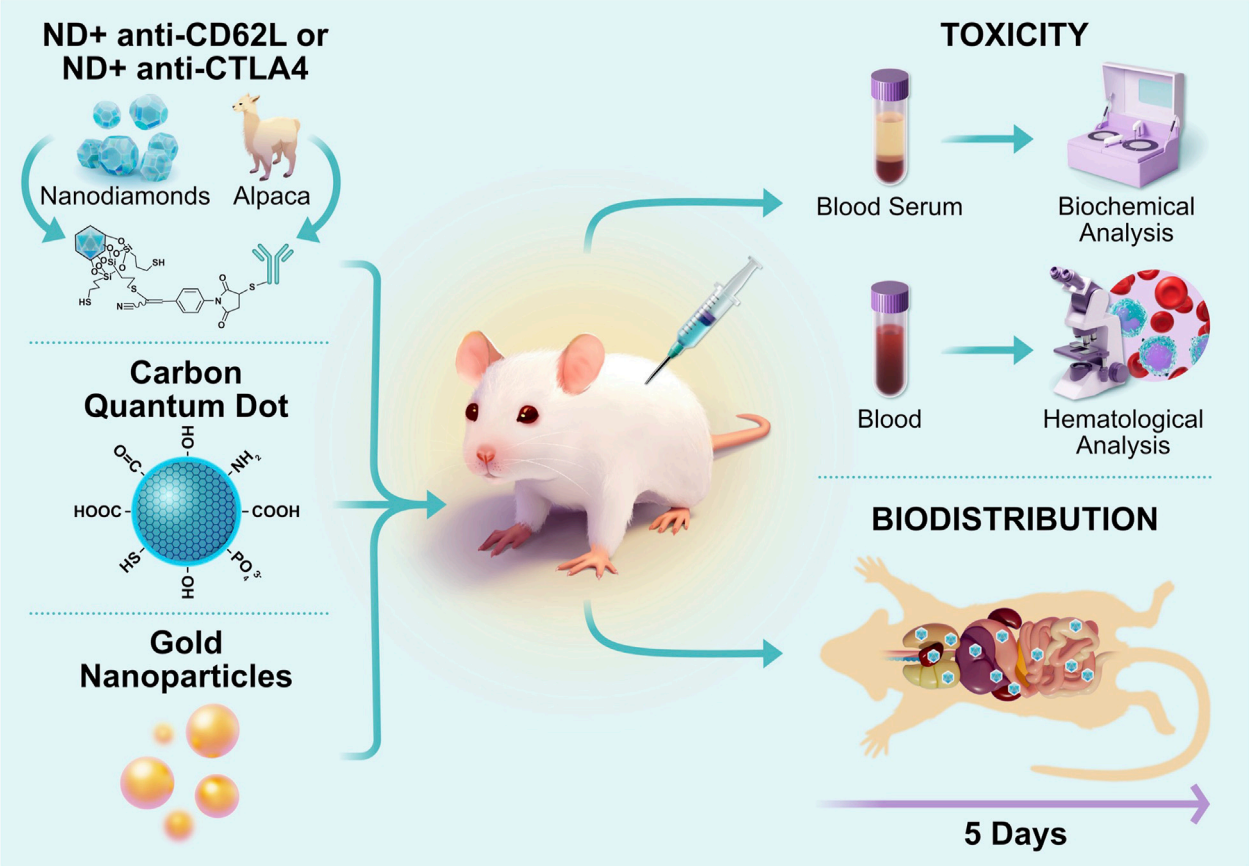

FIGURE 1
Toxicity and biodistribution analysis of functionalized nanoparticles in a mouse model.

Fluorescent-labeled nanoparticles, such as quantum dot nanocarbons, are essential tools in biomedical research, with applications in in vitro cell labeling and *in vivo* imaging (Xing and Dai, 2009). However, their safety is still debated and is influenced by factors like surface coating, size, and surface charge. Most current safety assessments are based on *in vitro* studies, and further validation in animal models is necessary to confirm their safety *in vivo*.

1.2 Nanodiamond biodistribution

The efficacy and toxicity of nanoparticles are significantly influenced by their biodistribution profile and exposure at the site of action (Kumar et al., 2023). Despite preclinical studies evaluating nanoparticle biodistribution, most focus on determining the pharmacokinetics (PK) of drugs loaded within the nanoparticles rather than the particles themselves. Understanding *in vivo* biodistribution trends of different nanoparticles is critical to determining how their properties affect PK (Kumar et al., 2023).

Results show that after intravenous injection, nearly 60% of NDs accumulate in the liver, followed by the spleen and lungs, with smaller amounts distributed to other organs. NDs can also be excreted through the bladder/urinary tract for clearance (Yuan et al., 2009). Since NDs elicit immune responses differently in animal models, it would be valuable to evaluate their biodistribution at multiple concentrations *in vivo* and compare these results with other promising nanomaterials (Puzyr et al., 2007).

1.3 Evaluating the efficacy of nanodiamond-delivered nanobodies via flow cytometry

Flow cytometry is a valuable tool for evaluating T-cell activation and immunosuppression, as it can measure several cellular activation parameters such as cytokine and adenosine triphosphate (ATP) upregulation, as well as T-cell proliferation (Zappasodi et al., 2020). Cytokines and ATP are key mediators of ND–immune system interactions. Elevated cytokine levels (e.g., IFNγ, TNFα, and IL-6) typically indicate an active immune response, often due to inflammation or infection, whereas low levels suggest immunodeficiencies or a dysregulated immune response (Iwamoto et al., 2014). ATP, considered the "energy currency" of the cell, influences numerous cellular processes. High ATP levels may indicate a potential stress response or increased metabolism, while low levels suggest impaired metabolism or depleted energy stores (Shao et al., 2018; Di Virgilio et al., 2018). Therefore, examining changes in cytokine secretion and ATP levels can provide insight into the mechanisms through which NDs interact with cellular factors.

In this study, we also evaluated T-cell populations and subpopulations, as T-cells play a crucial role in host defense. Treatment with NDs has been shown to counteract age-associated declines in splenic $CD4^+$ and $CD8^+$ T cells in mice (Ghoneum et al., 2010). Thus, we hypothesized that immune system activation and T-cell populations would increase in the ND + anti-CD62L and ND + anti-CTLA4 groups, but not in other groups.

Nanobodies, which are single-domain antibodies, are the smallest fragments of antibodies capable of binding antigens with affinities comparable to conventional antibodies. Due to their low tendency to aggregate, improved tissue penetration, and ability to label thicker tissue segments, nanobodies have broad applications in therapeutics and imaging. In this study, we incorporated nanobodies (purchased from NanoTag Biotechnologies) as targeting ligands. Specifically, we chose anti-CD62L and anti-CTLA4 nanobodies because they provide precise, targeted, and effective treatment—particularly for leukemia and solid tumors—by inducing selective apoptosis, enhancing adoptive immunotherapy, and improving checkpoint inhibitor responses (Burgess et al., 2013). Therefore, flow cytometry was performed to evaluate whether the nanobodies remained active after delivery via NDs, and whether they successfully activated the immune system. These results would support the potential of ND-based delivery systems, especially for targeting lymph nodes, where T cells are activated (Harris et al., 2002).

1.4 Findings and overview

In vivo systems are complex, and a comprehensive evaluation and comparison of various nanoparticles (NPs) at different concentrations and time points is crucial (Fischer and Chan, 2007). NPs interact with the host's immune system, resulting in either immunosuppression or immunostimulation, ultimately influencing their effects. Understanding these interactions is essential to optimize treatment benefits and minimize toxicities (Song et al., 2014). Therefore, the present study evaluated the dose-dependent toxicity and biodistribution patterns of NPs in C57BL/6 mice.

Cytokine analysis revealed that gold nanoparticles and ND + anti-CD62L treatments significantly elevated IL-6 and TNF-α levels at 2 hours post-dosing, indicating an inflammatory response. Biodistribution analysis showed that NDs accumulated persistently in the heart, gold nanoparticles in the left lung, and quantum dot nanocarbons in the kidney, with transient presence in other organs. Gold nanoparticle treatment resulted in the highest activation of memory T cells, suggesting immune system activation.

In conclusion, while gold nanoparticles induced significant inflammatory responses and quantum dot nanocarbons activated memory T cells, control ND treatment exhibited a more favorable profile, with lower inflammatory responses and no significant activation of memory T cells. Therefore, ND treatments demonstrated superior tolerability and a more controlled immune response under the conditions of this study. These results provide key insights and contribute to a better understanding of the potential benefits and health risks of nanoparticle-based therapies.

2 Materials and methods

2.1 Study design

This study investigated the effects of various treatments on mice, sorted by body weight into 22 groups, each receiving a single

TABLE 1 Study design as of Day 1 of the study.

Group	n	Treatment regimen			
		Agent	mg/kg	Route	Schedule
1	3	No Treatment	---	---	---
2	3	vehicle	---	iv	Day 1
3	3	Control ND	5	iv	Day 1
4	3	Control ND	10	iv	Day 1
5	3	Control ND	20	iv	Day 1
6	5	Control ND	40	iv	Day 1
7	3	Gold nanoparticles	5	iv	Day 1
8	3	Gold nanoparticles	10	iv	Day 1
9	3	Gold nanoparticles	20	iv	Day 1
10	5	Gold nanoparticles	40	iv	Day 1
11	3	Nanocarbon quantum dot	5	iv	Day 1
12	3	Nanocarbon quantum dot	10	iv	Day 1
13	3	Nanocarbon quantum dot	20	iv	Day 1
14	5	Nanocarbon quantum dot	40	iv	Day 1
15	3	ND + anti-CD62L	5	iv	Day 1
16	3	ND + anti-CD62L	10	iv	Day 1
17	3	ND + anti-CD62L	20	iv	Day 1
18	5	ND + anti-CD62L	40	iv	Day 1
19	3	ND + anti-CTLA4	5	iv	Day 1
20	3	ND + anti-CTLA4	10	iv	Day 1
21	3	ND + anti-CTLA4	20	iv	Day 1
22	5	ND + anti-CTLA4	40	iv	Day 1

intravenous dose. Mice were administered control ND, gold nanoparticles, quantum dot nanocarbons, ND + anti-CD62L, or ND + anti-CTLA4 at concentrations of 5, 10, 20, or 40 mg/kg. The selection of 5, 10, 20, and 40 mg/kg doses was guided by a combination of preclinical nanotoxicology principles and literature precedence (Yuan et al., 2009; Aillon et al., 2009b; Hare et al., 2017; Caron et al., 2012). This incremental approach spanned from potentially sub-toxic levels (5 mg/kg) to a higher threshold (40 mg/kg) to uncover any emerging toxicity signals. Indeed, most formulations remained within acceptable tolerability limits across these doses, with no group exceeding the 20% mean body weight loss criterion. Notably, two animals in the 40 mg/kg ND + anti-CD62L cohort exhibited acute respiratory distress, suggesting that 40 mg/kg may serve as an upper limit for this particular functionalized formulation (Alexander and Leong, 2024; Lundqvist et al., 2008). Transient elevations in IL-6 and TNF-α were seen at 40 mg/kg with certain gold and nanodiamond conjugates, aligning with prior studies showing that mid-to-high double-digit mg/kg doses often provoke pronounced inflammatory and organ-accumulation patterns (Hammami et al., 2021; Aillon et al., 2009b; Khan et al., 2020). To refine these observations and better delineate dose-response trends, future experiments will incorporate midrange doses (e.g., 15 mg/kg, 30 mg/kg) and extended observation windows, thereby enabling a more thorough assessment of delayed-onset toxicities, immune activation dynamics, and formulation-specific safety profiles (Fischer and Chan, 2007; Blanco et al., 2015). Serum cytokines, blood samples, organ biodistribution, and changes in T-cell subpopulations were analyzed over the course of 5 days. Treatment tolerability was assessed through body weight measurements and regular monitoring for clinical signs of treatment-related side effects. Terminal samples were collected for biodistribution, flow cytometry, and cytokine analyses (Table 1).

Vehicle = 10 mM Potassium Phosphate pH 7.2 + 0.5% PEG1.5k in PBS.

In selecting the specific doses (5, 10, 20, and 40 mg/kg) and time points (2, 24, and 96 h), we aimed to capture a comprehensive range of nanoparticle behaviors and responses *in vivo*. These dose levels were chosen to represent a gradient from low, potentially sub-toxic concentrations to higher doses that could reveal more pronounced biological effects or toxicity thresholds, aligning with established preclinical dose-escalation strategies and previous nanoparticle

studies (Aillon et al., 2009a; Kumar et al., 2023; Hare et al., 2017; Caron et al., 2012). The lowest doses provide baseline information on distribution and immune tolerance, while the higher doses probe the upper limits of tolerability and immunogenicity. Similarly, the three time points ensure coverage of immediate distribution and acute reactions (2 h), interim tissue retention and early clearance processes (24 h), and longer-term biodistribution patterns and potential delayed effects (96 h), thus offering a dynamic view of nanoparticle fate within the organism (Blanco et al., 2015; Reagan-Shaw et al., 2008).

In addition to characterizing toxicity and biodistribution within a murine model, it is essential to consider how these dosing regimens might be translated into a human clinical context. Although direct conversions are challenging due to physiological, metabolic, and immunological differences between species, established dose-scaling methods can provide a preliminary framework. For instance, approaches that normalize doses by body surface area or apply allometric scaling factors are commonly used to estimate human equivalent doses from animal data (Reagan-Shaw et al., 2008; Nair and Jacob, 2016). These methods account for differences in metabolism, blood volume, and organ function that often influence nanoparticle pharmacokinetics and pharmacodynamics (Kumar et al., 2023; Caron et al., 2012). Together, these strategies ensure that the preclinical findings not only serve as a robust guide for understanding nanoparticle behavior in animal models but also provide a foundational basis for future clinical translation and safe, effective dosing strategies in humans.

2.2 Background of therapeutic agents

Laser-synthesized nanodiamonds (LNDs) have gained popularity due to their higher purity (>94% carbon) and smaller diameter (4–7 nm) compared to other common NDs, such as detonation NDs (DNDs, 4–100 nm, <86% carbon) or high-temperature high-pressure NDs (HTHPNDs, ≥40 nm, irregular shape). LNDs also exhibit superior structural and spectroscopic properties, offer easier control over surface chemistry, demonstrate higher practical utility, and show minimal cytotoxicity, making them the preferred choice for our study (Alexander and Leong, 2024; Baidakova et al., 2013; Perevedentseva et al., 2015).

We aimed to develop a platform leveraging the small size and low toxicity of NDs to transport cargo or targeting agents. Nanobodies, also known as single-domain antibodies (sdAbs), were chosen as targeting agents due to their smaller size, ease of conjugation, and ability to cross the blood-brain barrier. Originating from the Camelidae family, nanobodies are isolated from alpacas and llamas, with a molecular weight of 12–15 kDa compared to conventional antibodies (~150 kDa). Although research on nanobodies spans three decades, their application has been limited by patents, which are now expiring, allowing for broader use.

In developing the ND platform, a standardized thiolation process was meticulously applied to enable efficient nanobody conjugation and additional functionalization steps. LNDs were treated with 3-mercaptopropyl trimethoxysilane (MPTMS) under controlled conditions, producing an average of four thiol groups per particle. By adjusting MPTMS levels, we achieved precise control over thiol density, ensuring a consistent thiolated surface for subsequent modifications, including the attachment of nanobodies, polyethylene glycol (PEG), and fluorophores. Following thiolation, unreacted reagents were removed through repeated centrifugation and washing in sterile-filtered ethanol, preserving the purity and functional integrity of the LNDs.

Cysteine-tagged nanobodies were then conjugated using APN-maleimide chemistry, allowing specific, mild attachment without disrupting their active sites. The maleimide group's rapid reactivity enabled stable nanobody linkage to the thiolated ND surface while maintaining functionality. To verify uniform thiolation and successful conjugation, Ellman's assay was performed, confirming an average of four thiols per ND.

For further functionalization, DBCO-PEG4-TAMRA and DBCO-mPEG2k were incorporated to facilitate tracking and enhance stability. TAMRA was chosen for its photostability, and PEG chains improved colloidal stability and minimized non-specific protein interactions. A controlled, sequential addition was employed for optimal loading: DBCO-TAMRA was introduced and allowed to react for 2 hours before DBCO-PEG was added. Dynamic Light Scattering (DLS) confirmed that this approach preserved ND stability and maintained consistent structural integrity (Figure 2).

This functionalization protocol provides a reproducible method to integrate nanobodies, PEG, and fluorophores onto the ND surface, creating a biocompatible, stable platform for targeted therapeutic delivery and biodistribution studies *in vivo*.

The figure illustrates the stepwise process for developing a fully functionalized ND prototype with targeting, imaging, and biocompatibility properties. Initially, thiol groups are introduced onto the ND surface through silanization, creating reactive sites for subsequent conjugation. A maleimide-activated linker (APN-maleimide) is then coupled to thiol-containing nanobodies via thiol-maleimide chemistry, generating a nanobody-linker conjugate. This APN-nanobody complex is attached to the thiolated ND surface, resulting in a targeted ND functionalized with a specific recognition element. To enable further modifications, azide groups are incorporated onto the surface, allowing bio-orthogonal click chemistry. Strain-promoted azide-alkyne cycloaddition (SPAAC) is then employed to conjugate a DBCO-functionalized fluorophore (TAMRA-PEG4-DBCO) for imaging and a PEG molecule (DBCO-mPEG2k) to enhance biocompatibility, stability, and minimize aggregation. The resulting ND prototype integrates targeting capabilities, fluorescent labeling for imaging, and PEGylation for improved performance in biological systems, offering a versatile platform for advanced biomedical applications.

Gold nanoparticles and quantum dot nanocarbon were obtained from Luna Nanotech and Nanopartz Inc., respectively. On the day of dosing, these materials were diluted in the provided vehicle (10 mM Potassium Phosphate, pH 7.2, with 0.5% PEG1.5k in PBS) to prepare solutions at 0.5, 1, 2, and 4 mg/mL, delivering doses of 5, 10, 20, and 40 mg/kg, respectively, when administered at 10 mL/kg.

2.3 Mice

Female C57BL/6 mice (C57BL/6 NCrl, approximately 10 weeks old, 18.5–24.6 g) were obtained from Charles River. The mice were provided with *ad libitum* access to water and NIH 31 Modified and

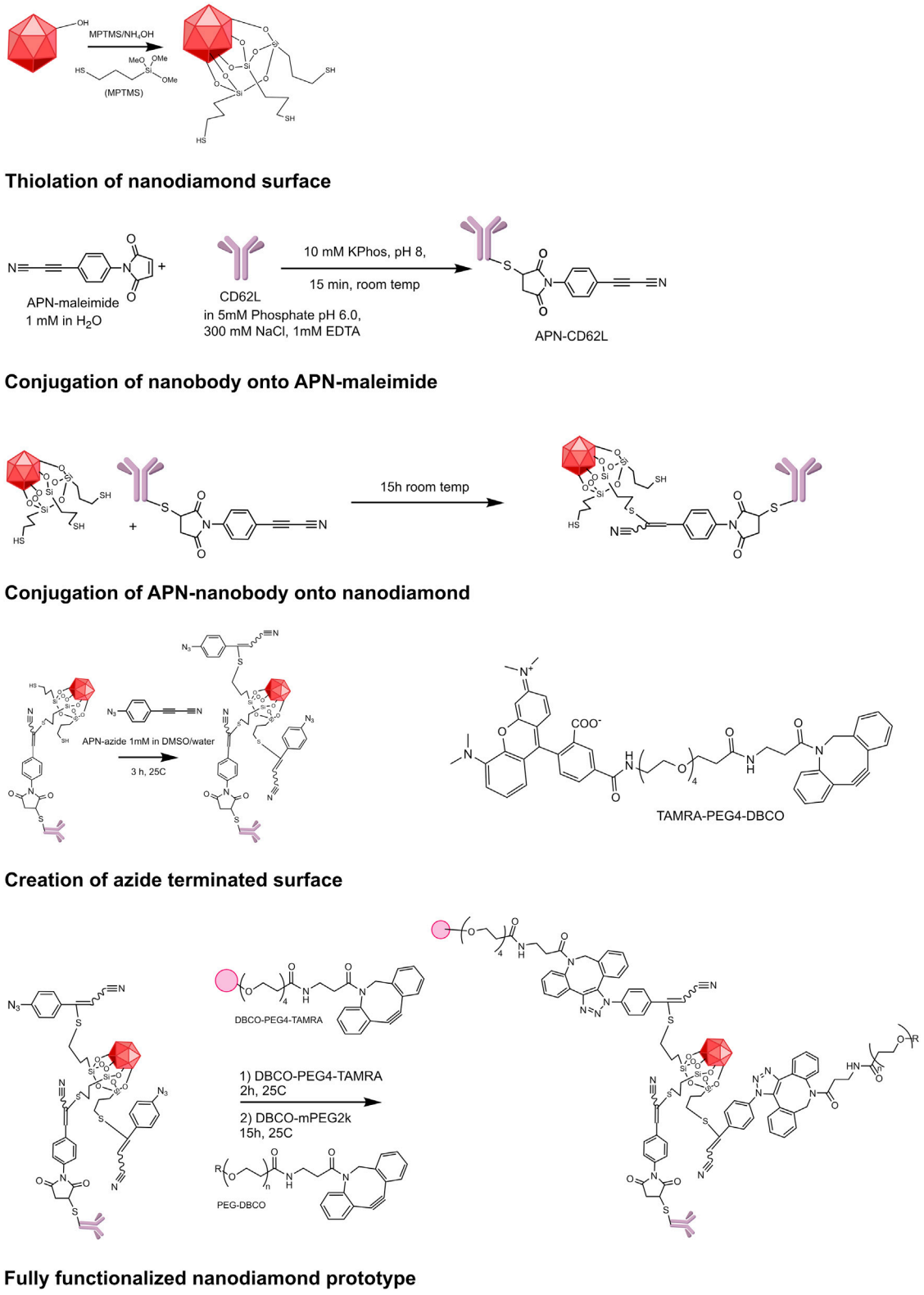

FIGURE 2
Schematic representation of nanodiamond surface functionalization for targeted and multifunctional applications.

Irradiated Lab Diet® until 1 week prior to study initiation, after which they were switched to an RD D10012Mi diet for the duration of the study. The animals were housed in irradiated Enrich-o'cobs™ bedding in static microisolators on a 14-hour light/10-hour dark cycle at 20°C–22°C (68°F–72°F) and 40%–60% humidity. All experiments involving mice were conducted in accordance with

the Guide for the Care and Use of Laboratory Animals and were compliant with the guidelines of the Association for Assessment and Accreditation of Laboratory Animal Care International (AAALAC).

2.4 Sorting and treatment

On Day 1, female nude mice were sorted by body weight (BW) into 22 groups, and dosing was initiated according to the treatment plan outlined in Table 1. All doses were administered intravenously (i.v.) once on Day 1.

2.5 Sampling

Blood and organ samples were collected and processed. Submental blood samples (~100 μL) were taken at 2 and 24 h post-dose from all animals in all groups, except for Groups 6, 10, 14, 18, and 22. Blood was processed for serum (≥50 μL) without anticoagulant and stored at −80°C. Thawed serum samples were assayed in duplicate at CRL-NC using the Luminex system (Millipore Cat. No. MCYTOMAG-70K) to measure interferon-gamma (IFN-γ), tumor necrosis factor-alpha (TNF-α), and interleukin-6 (IL-6) levels (for details, see Supplementary Information).

2.6 Biodistribution

Post-dose samples from the liver, stomach, spleen, left lung, left kidney, heart, feces, and blood were collected at 2 h (Sampling 2), 24 h (Sampling 5), and 96 h (Sampling 7) and stored at −80°C. Tetramethylrhodamine (TAMRA) was used to detect NDs, infra-red (IR) 750 for gold nanoparticles, and red fluorescence for quantum dot nanocarbons (for details, see Supplementary Information).

2.7 Flow cytometry

Whole blood samples were collected on Day 2 (24 h post-dose), cooled to 4°C, and processed for flow cytometry by erythrocyte removal using ACK buffer, followed by resuspension in PBS. Samples were analyzed for nine T-cell populations: total T cells, and total, naïve, central memory, and effector memory $CD4^+$ and $CD8^+$ T cells (for details, see Supplementary Information). Descriptive statistics and graphical presentations were generated using JMP17 software.

2.8 Tolerability

Animals were weighed daily from Days 1–5. Group mean BW nadirs were determined before more than 50% of the animals in a group exited the study. The mice were closely monitored for health and any overt treatment-related (TR) adverse effects, and clinical observations were recorded if noted. Acceptable toxicity was defined as a group mean BW loss of less than 20% during the study and no more than 10% TR mortality. Any dosing regimen resulting in greater toxicity was considered above the maximum tolerated dose (MTD). A death was classified as TR if it was attributable to treatment side effects as evidenced by clinical signs and/or necropsy findings or occurred due to unknown causes during the dosing period or within 14 days post-dosing.

Any animal with weight loss exceeding 30% in a single measurement or 25% for three consecutive measurements was euthanized and classified as a TR death. Deaths were classified as non-treatment-related (NTR) if there was no indication that the death was related to treatment side effects and occurred more than 14 days post-dosing. NTR deaths were further categorized as NTRa (due to accident or human error) or NTRu (due to unknown causes). It should be noted that treatment side effects were not excluded from deaths classified as NTRu.

GraphPad Prism 10.0.3 for Windows was used for graphical presentation of group mean BW loss from Day 1. Error bars indicate one standard error of the mean (SEM).

3 Results

3.1 Tolerability

3.1.1 Body weight changes

Animal body weights (BWs) were measured daily throughout the study. Across the treatment groups, maximum mean BW losses ranged from 0% (Groups 1, 2, 5, 11, 13, and 18) to 9.4% (Group 17 on Day 2). These variations fell within acceptable tolerability limits, as no groups exceeded the threshold of 20% mean BW loss.

3.1.2 Unscheduled deaths

Two treatment-related deaths occurred in Group 18 (40 mg/kg ND + anti-CD62L) on Day 1. Affected animals exhibited lethargy and labored breathing shortly after dosing and did not recover. Necropsy revealed mottled liver and lungs, suggesting immune-mediated organ damage. CD62L, a regulator of leukocyte migration, may have induced widespread immune cell activation, leading to systemic inflammation and subsequent organ failure. This highlights the potential risks of therapies targeting immune cell migration.

3.1.3 Changes in T-cell signatures

To evaluate immune modulation, whole blood samples were collected 24 h after dosing (Day 2). Flow cytometry assessed total T cells, including $CD4^+$ and $CD8^+$ subsets, and activation markers (CD69, CD25). Total T cells ($CD45^+$) comprised 40.7%–49.1% of the immune population.

Group 6 (ND) can be considered superior due to its moderate T cell response (Figure 3). An excessively high T cell percentage, as observed in Group 10 (Gold nanoparticles), may indicate overactivation of the immune system, which could result in adverse effects such as excessive inflammation or autoimmune reactions. Group 14 (Quantum dot nanocarbons) also exhibited higher immune activation compared to Group 6 (ND).

Of the total T cells, 55.9%–57.97% were $CD4^+$ and 37.83%–39.13% were $CD8^+$. The majority of both $CD4^+$ (75.9%–83.2% of parent) and $CD8^+$ (82.2%–87.2% of parent) T cells were naïve. Differential activation, as measured by CD25 expression, was observed in $CD4^+$ T cells, $CD8^+$ T cells, $CD8^+$ T central memory

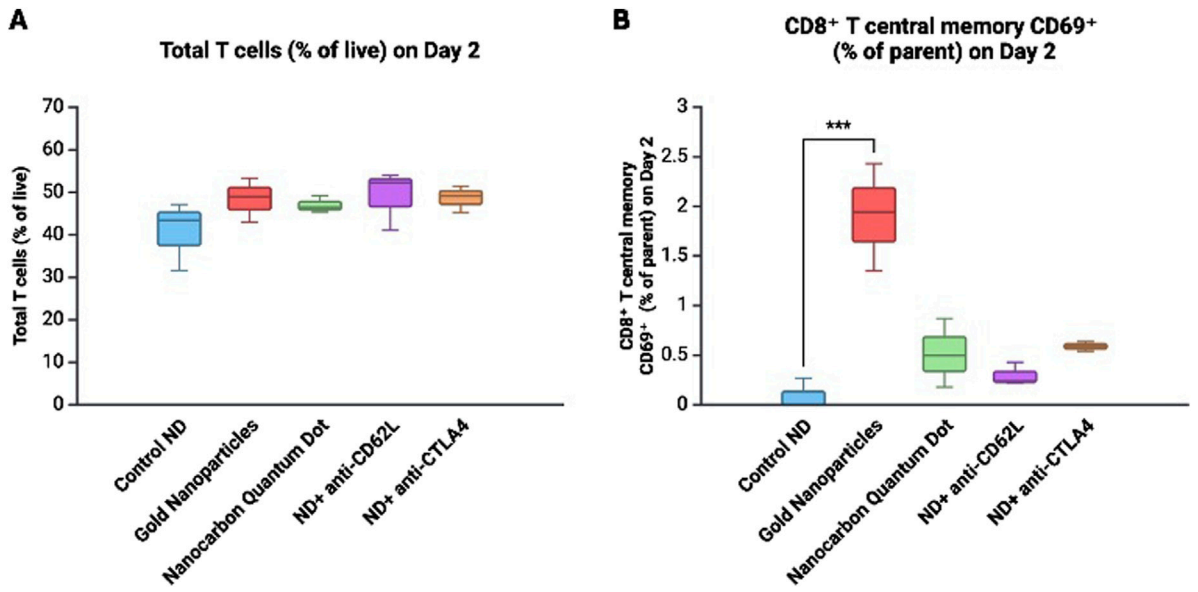

FIGURE 3
Effects of Nanoparticle Treatments on T-Cell Populations at Day 2 Post-Dosing: **(A)** shows the percentage of total T cells among live cells, allowing assessment of overall T-cell levels across treatment groups. **(B)** focuses on $CD8^+$ T central memory cells, a subset of T cells important for long-term immune memory. Here, CD69 expression is used as an early marker of activation, indicating how these memory cells respond to the treatments shortly after dosing. Central memory $CD8^+$ T cells play a crucial role in mounting rapid responses upon re-exposure to pathogens, and understanding their activation status (via CD69 expression) provides insights into how nanoparticles may influence immune readiness and memory formation. Values represent the mean ± SEM *p < 0.05 vs. control; **p < 0.01 vs. control; ***p < 0.001 vs. control; and ****p < 0.0001 vs. control.

cells (1.91% vs. 0.09%–0.59%), and $CD8^+$ effector memory cells (3.95% vs. 0.25%–0.7%) compared to other groups.

The elevation of $CD8^+$ T Central Memory $CD69^+$ (% of Parent) on Day 2 (Figure 3) is particularly concerning, as it suggests that these potent cytotoxic cells are being rapidly reactivated, potentially leading to immediate and significant immune-mediated damage if not properly regulated. $CD8^+$ T Central Memory cells are already primed to respond quickly upon re-exposure to their specific antigen. When they express CD69, it signals immediate activation, indicating they are prepared to carry out cytotoxic functions rapidly. If this activation is misdirected or excessive, it could result in severe tissue damage, autoimmunity, or exacerbation of chronic conditions due to the aggressive nature of $CD8^+$ T cells. These cells can directly kill target cells, and an overactive response can cause substantial harm. Group 6 (ND) shows the lowest activation level relative to the Quantum dot nanocarbons (Group 14) and Gold nanoparticles (Group 10).

While CD69 indicates immediate activation, CD25 expression suggests that the cells are primed for sustained activity. These cells may be proliferating and preparing for longer-term responses, such as memory cell expansion or prolonged cytotoxic activity (Figure 4). Elevated CD25 levels on central memory $CD8^+$ T cells could lead to prolonged activation and expansion of these cells, contributing to chronic inflammation if the immune response is not properly controlled.

Group 6 (NDs) outperformed Group 10 (Gold nanoparticles) and Group 14 (Quantum dot nanocarbons) in terms of immune response management. The moderate and consistent activation of $CD8^+$ T central memory cells suggests that NDs offer a more controlled and predictable immune activation, reducing the risk of overactivation and its associated adverse effects. In contrast, the higher and more variable activation observed in Groups 10 and 14 could lead to less favorable outcomes, making NDs the superior option among the groups tested.

The effects of nanodiamond-based treatments on T-cell subsets and activation markers were further assessed through heatmap analysis (Figure 5). The ND + anti-CTLA4 treatment led to a reduction in $CD4^+$ naïve T cells while increasing effector memory subsets, suggesting enhanced differentiation. $CD8^+$ naïve T cells also decreased, while central and effector memory populations remained stable or expanded, indicating sustained immune modulation. Additionally, ND + anti-CTLA4 enhanced $CD4^+$ effector memory activation, whereas ND + anti-CD62L promoted $CD8^+$ central memory proliferation, highlighting distinct immune responses driven by these treatments.

3.1.4 Inflammatory cytokine levels

Two hours after dosing, both IL-6 and TNF-α levels were elevated in response to treatment with 40 mg/kg Gold nanoparticles (Group 10) (Figure 6). However, these cytokine levels returned to, or were near, baseline/limit of quantitation at 24 h and 96 h post-dosing.

Temporal cytokine analysis revealed dynamic immune responses to nanodiamond-based treatments, as shown in (Figure 7). Early post-treatment (2 h) responses included elevated inflammatory markers, particularly IL-6 and TNF-α, in the nanocarbon quantum dot and ND + anti-CTLA4 groups. By 24 h, these responses stabilized, with IFN-γ showing sustained elevation in the ND + anti-CD62L group. At 96 h, cytokine levels declined overall, although residual IL-6 expression in the

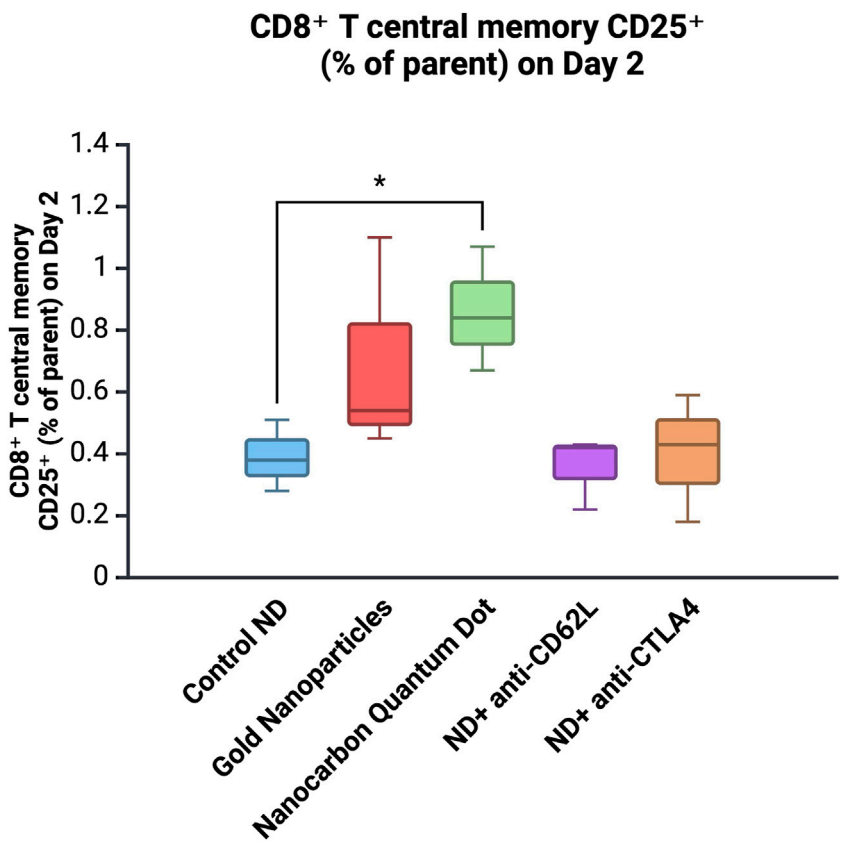

FIGURE 4
CD25 Expression on CD8⁺ T Central Memory Cells on Day 2 Post-Treatment: This figure illustrates CD25 expression as a percentage of the parent cell population across different nanoparticle treatment and control groups. CD25 is an activation marker associated with cell proliferation and immune response, helping to show how each treatment influences the activation status of CD8⁺ T central memory cells, which are vital for long-term immune memory and responsiveness. Values represent the mean ± SEM *p < 0.05 vs. control; **p < 0.01 vs. control; ***p < 0.001 vs. control; and ****p < 0.0001 vs. control.

ND + anti-CTLA4 group suggested prolonged immune activity. These results underscore the time-dependent immunomodulatory effects of nanodiamond treatments, with implications for controlling inflammatory responses and enhancing therapeutic efficacy.

3.2 Biodistribution

Tissue homogenates were collected at 2, 24, and 96 h after dosing and imaged using three excitation/emission wavelength settings optimized to detect TAMRA, IR, and red fluorophores (Figure 8). In TAMRA-detected ND groups (Groups 6: control, 18: anti-CD62L, and 22: anti-CTLA4), NDs persisted primarily in the heart at later time points, with short-term accumulation (elevated only at 2 h post-dosing) observed in the stomach, feces, spleen, liver, and left kidney for the control ND, and in the liver, blood, and left lung for anti-CTLA4.

Levels of IR-detected gold nanoparticles in Group 10 remained persistently high in the left lung, with transient and lower accumulation in the blood, left kidney, and liver. Red-detected quantum dot nanocarbons in Group 14 showed increased accumulation over time in the left kidney and a higher, but transient, presence in the liver, blood, and heart (Supplementary Appendix A).

Biodistribution analysis at 96 h post-treatment showed distinct organ-specific patterns across treatments (Figure 9). Control ND had the highest cardiac accumulation, while nanocarbon quantum dots and ND + anti-CTLA4 showed similar retention. Gold nanoparticles accumulated most in the lungs, and nanocarbon quantum dots had the highest liver retention, with faster clearance from blood. Fecal excretion and spleen retention were comparable across groups, highlighting the differential biodistribution and clearance dynamics of these treatments.

In comparing biodistribution profiles, several factors likely drove each nanoparticle to its predominant organ of accumulation. The relatively small hydrodynamic diameter and negative surface charge of nanodiamonds may allow them to circulate extensively and interact with cardiac vasculature or surrounding extracellular components, thus promoting heart-localized uptake (Haziza et al., 2017; Arvizo et al., 2011). In contrast, gold nanoparticles—often slightly larger or differently surface-modified—can become sequestered in the pulmonary capillary network, potentially influenced by alveolar–endothelial barriers or localized immune processes in lung tissue (Khan et al., 2020; Hauck et al., 2010). Quantum dot nanocarbons,

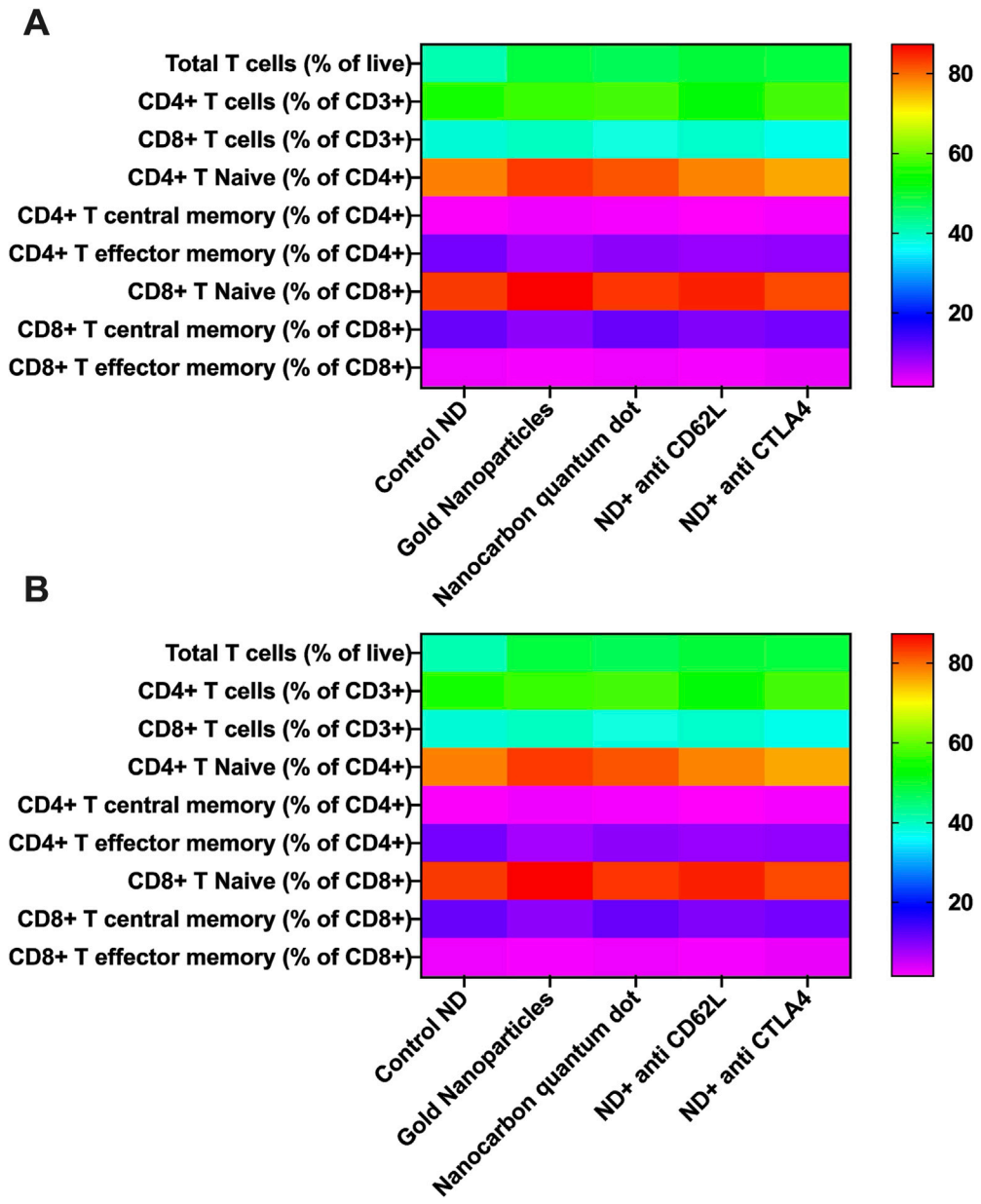

FIGURE 5
Heatmap analysis of T-cell populations and activation across experimental conditions: **(A)** Heatmap of T-cell population percentages. The ND + anti-CTLA4 treatment reduces $CD4^+$ naïve T cells while increasing effector memory subsets, suggesting enhanced differentiation. $CD8^+$ naïve T cells also decrease, while central and effector memory populations remain stable or increase, indicating nanodiamond-driven immune modulation. **(B)** Heatmap of T-cell activation markers. ND + anti-CTLA4 enhances $CD4^+$ effector memory activation ($CD69^+$, Ki67+), while ND + anti-CD62L drives increased proliferation in $CD8^+$ central memory subsets. These distinct activation patterns suggest differential immune responses based on the treatment applied. These findings demonstrate the potential of nanodiamond-based therapies to modulate T-cell populations and activation, offering promising implications for immunotherapy strategies.

being more hydrophilic and small enough for renal filtration, consequently display enhanced kidney retention alongside transient distribution to other organs (Xing and Dai, 2009; Longmire et al., 2008). These distinctive patterns highlight the necessity of carefully tailoring nanoparticle size, charge, and functionalization for specific clinical goals. From a translational standpoint, one might leverage gold nanoparticles' lung tropism for targeted pulmonary imaging or therapy, adapt nanodiamonds for cardiac drug delivery or regenerative applications, and cautiously exploit quantum dot nanocarbons' kidney accumulation for renal diagnostics or short-term imaging, provided toxicity concerns are rigorously addressed.

In addition to dictating organ-level tropism, nanoparticle size, surface chemistry, and functional moieties profoundly influence immune recognition and activation (Lundqvist et al., 2008; Cedervall et al., 2007). For instance, hydrophilic coatings (e.g., PEG) can attenuate protein corona formation and reduce phagocytic uptake, whereas conjugating nanobodies or antibodies

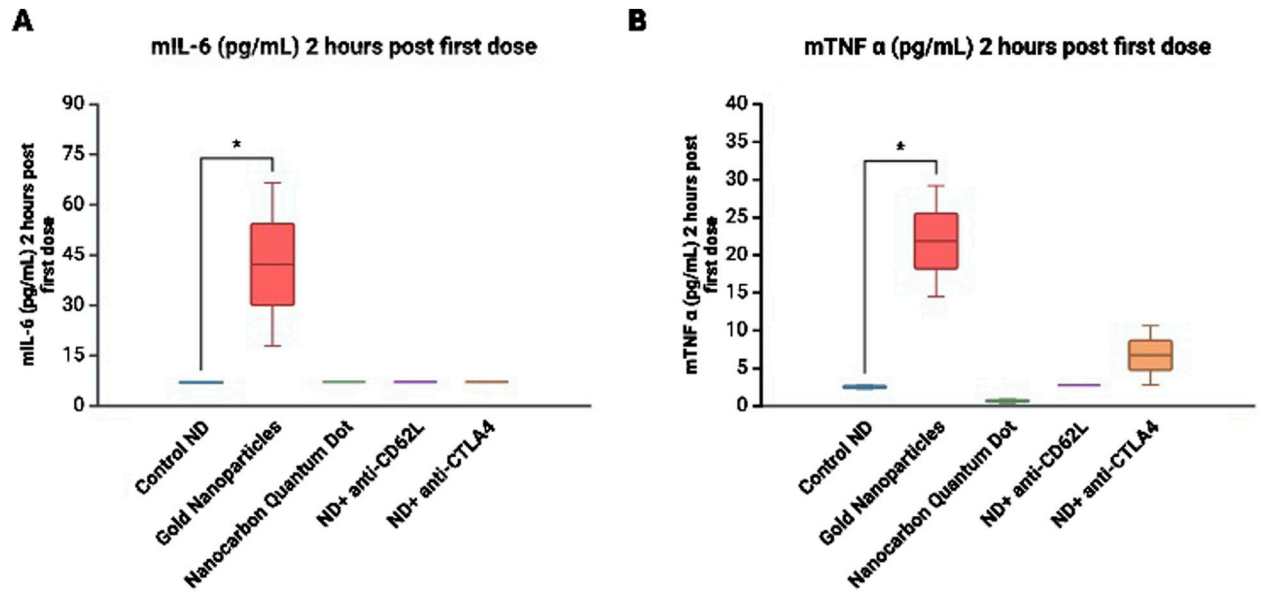

FIGURE 6
Concentration of mIL-6 (pg/mL) **(A)** and mTNF-α (pg/mL) **(B)** 2 Hours post-first dose: This figure displays levels of inflammatory cytokines mIL-6 and mTNF-α shortly after dosing, across various nanoparticle treatment and control groups. Elevated levels of these cytokines can indicate an immune response triggered by the treatment, offering insights into the early inflammatory effects of different nanoparticles. Values represent the mean ± SEM *p < 0.05 vs. control; **p < 0.01 vs. control; ***p < 0.001 vs. control; and ****p < 0.0001 vs. control.

may trigger receptor-mediated endocytosis and heightened T-cell activation (Arvizo et al., 2011). Subtle shifts in particle diameter or zeta potential can also affect how antigen-presenting cells process nanoparticle–protein complexes, leading to variable cytokine responses and immune cell proliferation (Xing and Dai, 2009; Albanese et al., 2012). In our study, these principles help explain why certain formulations (e.g., nanobody-conjugated nanodiamonds) elicited transient but notable immune activation, while others (e.g., unconjugated nanodiamonds) were relatively benign, underscoring the importance of precisely tailoring nanoparticle design for both safety and therapeutic efficacy.

Due to the relatively small sample sizes ($n < 5$) and the presence of non-normally distributed datasets, the non-parametric Kruskal–Wallis test was chosen for multi-group comparisons, ensuring robust inference without relying on normality assumptions. Preliminary checks (e.g., Shapiro–Wilk tests and QQ plots) indicated deviations from normality in several outcome measures, making the Kruskal–Wallis test more appropriate than ANOVA-based approaches. Where significant main effects were detected, Dunn's *post hoc* test was applied to pinpoint specific inter-group differences while controlling for Type I error inflation. Because this was an exploratory pilot study designed to identify broad safety margins and short-term biodistribution signals, a formal *a priori* power analysis was not conducted. Nonetheless, our sample sizes align with standard practice for initial nanotoxicology screens, and we plan to perform formal power analyses in subsequent studies to detect more subtle effects and better define long-term safety. For cytokine measurements (e.g., IL-6, TNF-α) conducted at 2, 24, and 96 h post-dosing, a multiplex magnetic bead-based Luminex® xMAP® platform was employed. This allowed for simultaneous quantification of multiple analytes with well-defined lower limits of quantitation—such as an mIL-6 LLOQ of 7.202 pg/mL—enhancing the sensitivity and reliability of the observed immune responses. Flow cytometry analyses of immune cell subsets (e.g., CD4+/CD8+ T cells, and markers like Ki67, CD25, and CD44) were summarized using descriptive statistics and graphically represented through box-and-whisker plots with individual data points. These plots, generated using JMP17 software, provided intuitive, high-resolution visualizations of median values, interquartile ranges, and outliers. For body weight and mortality data, criteria such as <20% mean weight loss and <10% treatment-related mortality were established as objective thresholds of tolerability. These data were depicted with standard error of the mean (SEM) error bars to convey variability and help assess the clinical relevance of our findings. In biodistribution analyses, fluorescence intensities were normalized to radiant efficiency units ($[p/s]/[\mu W/cm^2]$) to allow accurate comparisons over time (2, 24, and 96 h) and among tissues. While the small group sizes inherently limit statistical power and generalizability, these carefully selected and rigorously applied statistical and analytical methods collectively enhance the reliability, interpretability, and reproducibility of our findings, providing a stronger foundation for future research and potential clinical translation.

4 Discussion

4.1 Results interpretation

Nanoparticles (NPs) have gained popularity in biological applications, yet concerns about their *in vivo* toxicity persist. The present study aimed to evaluate the safety profile and biodistribution

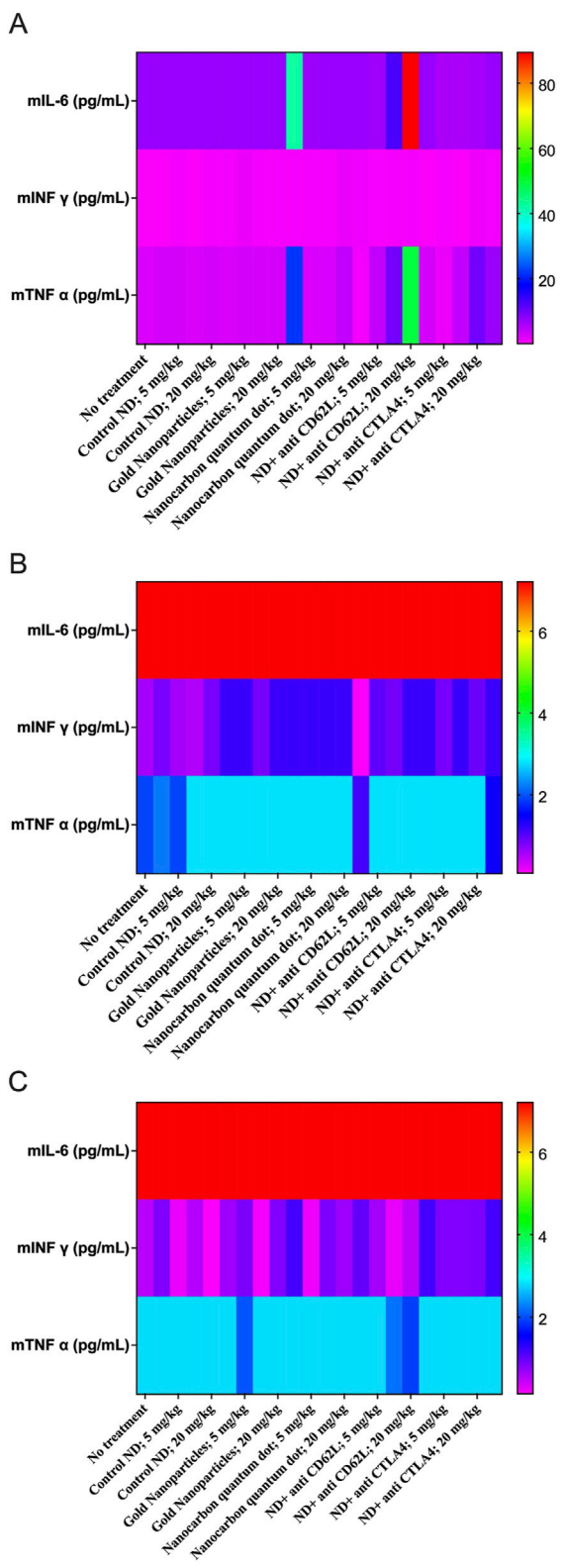

FIGURE 7
Heatmap analysis of cytokine levels across experimental conditions and Time points: **(A)** Heatmap of cytokine levels at 2 h post-treatment. The results show elevated IL-6 and TNF-α levels, particularly in the nanocarbon quantum dot and ND + anti-CTLA4 treatment groups, indicating an acute inflammatory response to these conditions. **(B)** Heatmap of cytokine levels at 24 h post-treatment. At this time point, cytokine levels begin to stabilize. IFN-γ

(*Continued*)

FIGURE 7 (Continued)
remains moderately elevated in the ND + anti-CD62L group, while TNF-α levels decrease across most treatments. IL-6 remains elevated in specific treatment groups, suggesting ongoing immune activation. **(C)** Heatmap of cytokine levels at 96 h post-treatment. Cytokine levels decline further, with residual IL-6 expression observed in the ND + anti-CTLA4 group, suggesting prolonged immune modulation. TNF-α and IFN-γ levels are significantly reduced, reflecting the resolution of early immune activation. These heatmaps highlight temporal cytokine response patterns under various treatment conditions, showcasing the distinct immune-modulatory effects of nanodiamond-based therapies.

patterns of various nanoparticle formulations, including Gold nanoparticles, Quantum dot nanocarbons, ND + anti-CD62L, and ND + anti-CTLA4. Samples were collected at multiple time points to assess organ- and time-dependent distribution. Data from blood, feces, and six different organs were included for detailed biodistribution analysis. The inclusion of appropriate controls, varying concentrations, and a rigorous dosing and monitoring process ensured a comprehensive assessment of safety and biodistribution. By tracking changes in body weight, cytokine levels, and T-cell populations, this study provides valuable insights into the effects of different NPs on the immune system.

Following intravenous (i.v.) administration, NPs first interact with the blood and its components. Being particulate materials similar in size to large proteins or viruses, NPs could induce an inflammatory response, potentially affecting immune system function and hematological factors (Hauck et al., 2010). Our study observed differential cytokine responses to NDs and other nanoparticles, with elevated secretion of IL-6 and TNF-α at 40 mg/kg Gold nanoparticles, and at 10 and 20 mg/kg ND + anti-CD62L, which returned to baseline levels at 24 and 96 h post-dosing. NPs also impacted T-cell responses, with NDs showing superior results due to a more moderate T-cell response compared to Gold nanoparticles and Quantum dot nanocarbons. T cells appeared sensitive to specific activation, as indicated by the IL-6 and TNF-α elevations in response to ND + anti-CD62L.

The biodistribution patterns varied with the type of NP used. Our results showed that 40 mg/kg control, anti-CD62L, and anti-CTLA4 NDs primarily accumulated in the heart. Short-term accumulation of control NDs was observed in the stomach, feces, spleen, liver, and left kidney, while anti-CTLA4 NDs were detected in the liver, blood, and left lung. Gold nanoparticles showed the highest levels in the left lung, whereas Quantum dot nanocarbons exhibited increased accumulation over time in the left kidney.

The analysis of mIL-6 levels at 2 h post-dosing revealed a statistically significant difference between Group 2 (G2) and the other groups, with a p-value of 0.0438 and a Kruskal–Wallis statistic of 33.23. The analysis of mTNF-α levels at 2 h also showed significant differences compared to other groups, with a p-value of 0.0021. These findings suggest a strong early response in mTNF-α levels, indicating meaningful variations across the experimental conditions at this time point. No significant differences were detected for the other cytokine (mINF-γ) or at later time points (24 and 96 h), suggesting that the early response (2 h) may be crucial for detecting cytokine differences in our study, with mIL-6 and mTNF-α being particularly responsive.

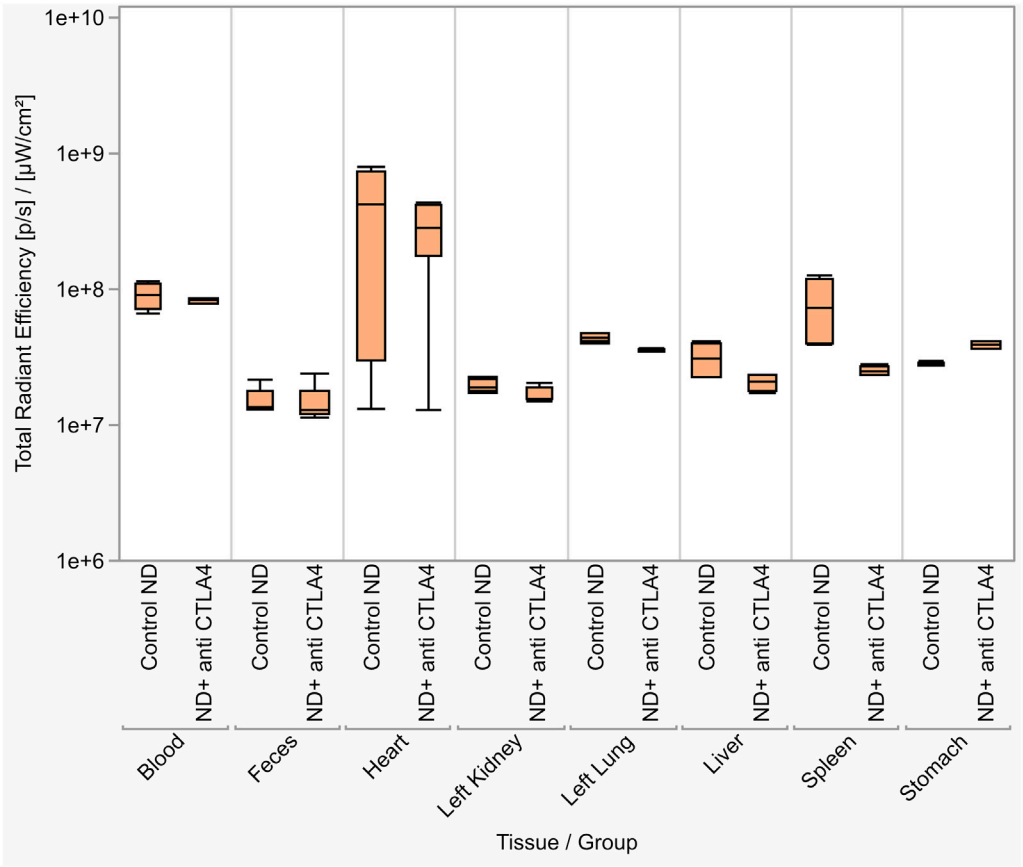

FIGURE 8
Biodistribution of nanoparticles at 40 mg/kg: total radiant efficiency in key organs at 96 hours post-first dose. This figure presents the biodistribution of NDs and ND combined with anti-CTLA4 across various tissues at 96 h post-first dose. The total radiant efficiency (p/s/µW/cm^2) is plotted on a logarithmic scale. Tissues analyzed include blood, feces, heart, kidney, lung, liver, spleen, and stomach. Notably, ND + anti-CTLA4 shows higher signals in the spleen and heart compared to controls, indicating significant tissue accumulation. Values represent the mean ± SEM *p < 0.05 vs. control; **p < 0.01 vs. control; ***p < 0.001 vs. control; and ****p < 0.0001 vs. control.

In line with recent high-profile research, we present a comprehensive toxicity and biodistribution assessment of functionalized NDs, quantum dot nanocarbons, and gold nanoparticles, emphasizing their immunomodulatory effects *in vivo*. Investigations into the surface engineering and physicochemical optimization of gold nanoparticles have highlighted how nuanced design choices can modulate biological activity (Chew et al., 2022). Innovative approaches like transient mild photothermia have further demonstrated that controlled conditions can enhance nanomedicine efficacy (Ma et al., 2024), while chain-like gold nanoparticle clusters have showcased improved imaging for neovascularization (Nguyen et al., 2023). In parallel, developments in ND research—including antibody quantification (Patil et al., 2021), enhanced quantum sensing (Shulevitz et al., 2024), quantum measurement for intracellular tracking (McGuinness et al., 2011), fluorescence-based transport analyses (Haziza et al., 2017), and targeted immune cell activation (Suarez-Kelly et al., 2021)—underscore their versatility and safety profile. Our findings reinforce these observations, revealing that NDs induce lower inflammatory cytokine secretion and reduced T-cell overactivation compared to gold nanoparticles and quantum dot nanocarbons. Moreover, the preferential accumulation of NDs in cardiac tissue, as opposed to the lung specificity of gold nanoparticles or kidney persistence of quantum dot nanocarbons (Haziza et al., 2017), highlights how properties such as surface charge, core composition, and ligand conjugation dictate organ-level distribution. By integrating these principles and corroborating the immunological benefits of NDs, we contribute new insights toward designing safer, more effective nanomedicines.

The observed differences in immune response and biodistribution can be attributed to the role of surface modifications in modulating nanoparticle interactions with immune cells. Surface properties, including charge, hydrophilicity, and functional groups, influence the formation of a protein corona, which determines immune cell recognition and response (Cedervall et al., 2007). Hydrophilic coatings, such as polyethylene glycol (PEG), reduce protein adsorption and minimize opsonization, leading to decreased phagocytic uptake and inflammatory responses, as observed with unconjugated NDs in this study. Conversely, nanobody-conjugated NDs

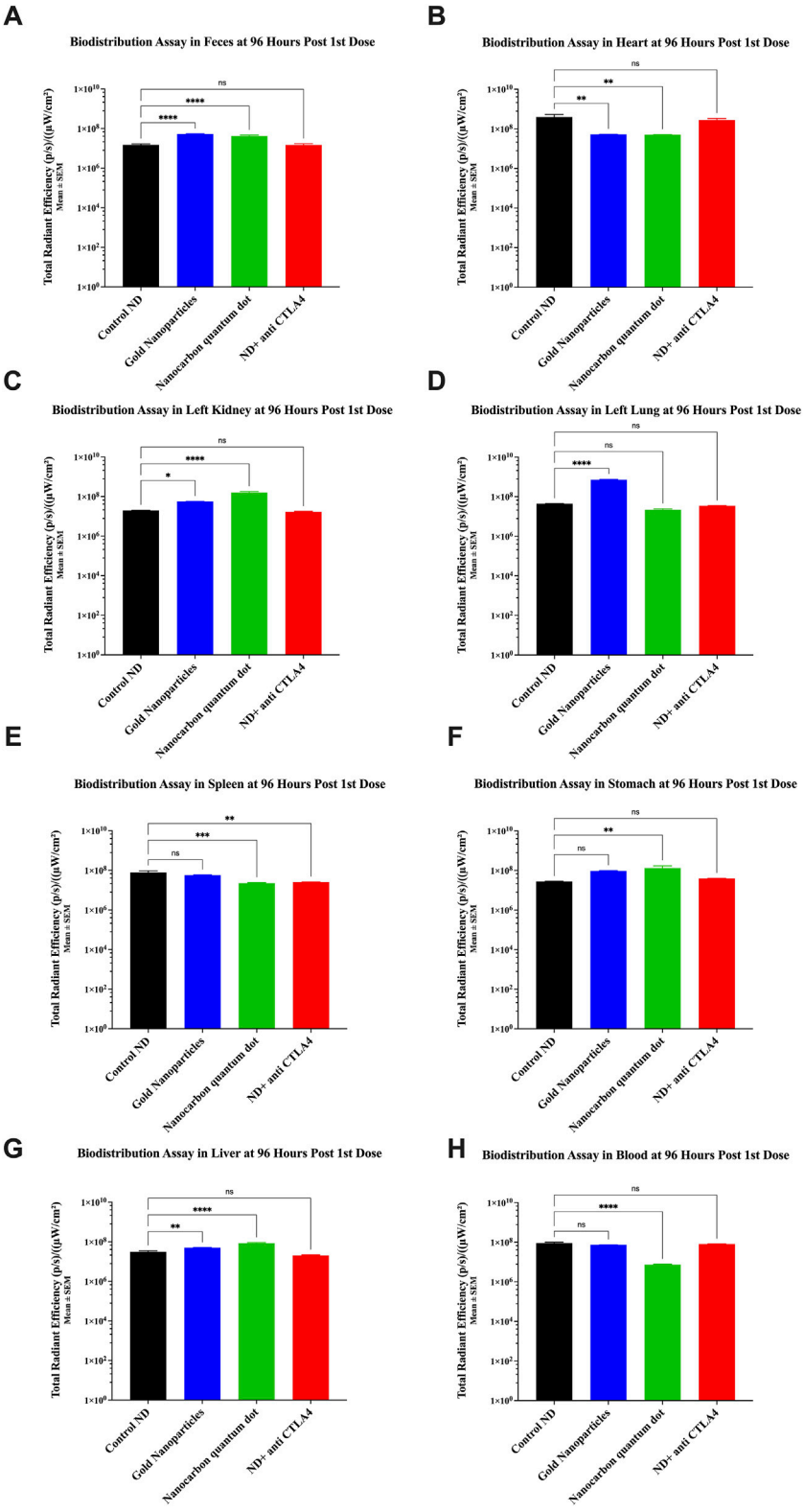

FIGURE 9
Biodistribution analysis at 96 hours post-treatment: **(A)** Biodistribution in feces. The total radiant efficiency levels are comparable across all treatment groups, with no significant excretion differences observed. **(B)** Biodistribution in the heart. Control ND exhibits the highest signal, while nanocarbon quantum dot and ND + anti-CTLA4 treatments show similar retention, suggesting potential cardiac accumulation. **(C)** Biodistribution in the left kidney. Gold nanoparticles and nanocarbon quantum dots show slightly increased retention compared to control ND, while ND + anti-CTLA4 remains stable. **(D)** Biodistribution in the left lung. Gold nanoparticles demonstrate the highest accumulation, whereas control ND and nanocarbon quantum dots show lower retention levels. **(E)** Biodistribution in the spleen. All treatment groups exhibit comparable levels, with minor variations between nanocarbon-based treatments. **(F)** Biodistribution in the stomach. No major differences are observed, indicating minimal gastrointestinal retention
(*Continued*)

FIGURE 9 (Continued)
variability across treatments. **(G)** Biodistribution in the liver. Nanocarbon quantum dots exhibit the highest retention, while ND + anti-CTLA4 shows slightly lower accumulation. **(H)** Biodistribution in blood. A reduction in total radiant efficiency is observed in nanocarbon quantum dot treatment, suggesting faster clearance from circulation compared to other groups. These findings provide insight into the biodistribution patterns of nanocarbon-based treatments, highlighting organ-specific accumulation and clearance dynamics over time. Values represent the mean ± SEM *p < 0.05 vs. control; **p < 0.01 vs. control; ***p < 0.001 vs. control; and ****p < 0.0001 vs control.

likely engage specific immune receptors, such as Fc or Toll-like receptors, facilitating receptor-mediated endocytosis and transient immune activation, evidenced by early cytokine secretion (Lundqvist et al., 2008). Biodistribution patterns further underscore the impact of surface modifications. NDs' cardiac accumulation may reflect charge- and size-mediated interactions with cardiac vasculature (Arvizo et al., 2011), while gold nanoparticles' retention in the lungs suggests capillary sequestration driven by size and hydrophobicity (Albanese et al., 2012). Similarly, quantum dot nanocarbons exhibited kidney accumulation, likely due to hydrophilic surface coatings favoring renal filtration and retention (Longmire et al., 2008). These findings demonstrate that surface modifications dictate immune recognition, uptake, and clearance pathways, which collectively shape immune responses and biodistribution profiles. Understanding these mechanisms is critical for designing nanoparticles with optimized therapeutic efficacy and minimal immunogenicity.

We acknowledge the limitation of using a single animal model (C57BL/6 mice) in this study, as it may not fully capture interspecies differences in nanoparticle biodistribution, immune responses, and toxicity. Rodent-specific clearance mechanisms and immune physiology may differ significantly from those in humans, potentially limiting the translational relevance of our findings. Additionally, while our study focused on acute toxicity and biodistribution, longer-term studies are needed to assess chronic toxicity and nanoparticle accumulation. Future research should include additional animal models, such as rats or non-human primates, to evaluate cross-species variability, extend observation periods to capture chronic effects, and explore different administration routes. Addressing these limitations will enhance the robustness and translational potential of nanoparticle-based therapies.

The observation periods in this study (2, 24, and 96 h post-dosing) were selected to capture immediate distribution, initial clearance, and short-term retention patterns, providing critical insights into nanoparticle behavior and immune response. Recognizing the importance of longer-term studies for understanding chronic toxicity, clearance mechanisms, and potential delayed effects, future investigations will include extended observation periods, such as weekly intervals over several months, to comprehensively assess long-term biocompatibility and safety. These findings serve as a foundation for further research into the long-term implications of nanoparticle use.

To address the gaps identified in this study, future research should focus on several key areas. First, extending observation periods to include long-term evaluations is critical for understanding chronic toxicity, nanoparticle clearance, and potential cumulative effects. Incorporating weekly or monthly intervals over extended durations would provide a comprehensive picture of nanoparticle persistence and long-term safety. Second, expanding the scope to include additional animal models or human-relevant systems would enhance the translational value of the findings and provide insights into interspecies variability in toxicity and biodistribution. Third, further studies should explore the impact of varied nanoparticle surface modifications, sizes, and functionalizations on immune interactions and clearance mechanisms. These efforts could also include advanced imaging techniques for real-time monitoring of nanoparticle dynamics *in vivo*. Collectively, such investigations will bridge current knowledge gaps and support the development of safer and more effective nanoparticle-based therapies.

4.2 Literature comparison

Previous studies have highlighted the association between pro-inflammatory cytokine expressions and nanoparticle material, size, concentration, and surface modification. Studies have reported no TNF-α secretion in mice with up to 25 mg/kg ND injection, and no immunogenicity with air-oxidized DND treatment up to 2.5 μM in chicken embryos (Tsai et al., 2016; Lazovic et al., 2024). Gold nanoparticles of 5–50 nm size have been found to cause a transient increase in IL-6 in rats and mice, with smaller sizes eliciting a minimal response compared to larger ones (50 nm) (Khan et al., 2020). Surface chemistry also plays a crucial role in determining the immunogenicity and cytotoxicity of nanoparticles. Prior research has demonstrated that IgG-conjugated LNDs induce pro-inflammatory responses at higher concentrations, underscoring the fine balance between nanoparticle functionalization and immune compatibility, which is important for targeted treatments (Alexander and Leong, 2024). Our results also highlight the role of surface chemistry and ND-nanobody conjugation in immune activation. This could be applied in the biomedical industry by designing specific surface modifications of NDs to elicit targeted immunological reactions.

Our study shows that 40 mg/kg control, anti-CD62L, and anti-CTLA4 NDs primarily accumulated in the heart, which differs from previous studies that reported higher localization of NDs in the liver after i. v. injection in mice and in the lungs after intratracheal injection (Tsai et al., 2016). We also observed short-term accumulation of control NDs in the stomach, feces, spleen, liver, and left kidney, and of anti-CTLA4 NDs in the liver, blood, and left lung. While Gold nanoparticles have previously been reported to localize to the liver and spleen, our study showed the highest levels in the left lung. Increased accumulation of Quantum dot nanocarbons was observed in the left kidney, which

aligns with findings from previous studies (Kumar et al., 2023; Hauck et al., 2010).

Our findings both corroborate and extend recent work on nanoparticle toxicity and biodistribution patterns *in vivo* (Sangabathuni et al., 2017; Bailly et al., 2019; Yang et al., 2017). For instance, shape and surface modifications of gold nanoparticles can significantly influence toxicity (Sangabathuni et al., 2017). Meanwhile, laser-synthesized AuNPs often exhibit minimal acute toxicity and predictable clearance (Bailly et al., 2019); however, our data reveal unexpected lung retention for certain formulations. Although repeated intravenous administration typically leads to substantial uptake in the liver and spleen (Yang et al., 2017), we observed distinct patterns in our study—particularly the notable accumulation of NDs in the heart and quantum dot nanocarbons in the kidney. These results underscore the importance of thorough, formulation-specific assessments to capture nanoparticle toxicity and organ-level fate accurately.

4.3 Applications and future research

Our study highlights the potential of NDs in biomedical applications, as they did not evoke significant inflammation or cytotoxicity. Surface modifications of NDs can be tailored for specific applications. For example, chemical functionalization can improve the attachment of drugs, ligands, or other molecules of interest; polymer coatings can enhance stability and biocompatibility; biomolecule conjugation can facilitate site-specific drug delivery; and surface charge modification can optimize drug loading, stability, and cellular uptake (Singh and Ray, 2023). Our results support conjugating NDs with nanobodies for a safe and precise treatment approach to target specific organs, tissues, and cells. LNDs possess inherent fluorescence and biocompatibility, making them crucial in bioimaging for non-invasive monitoring of disease progression and treatment response (Alexander and Leong, 2024). This study supports further exploration of ND biocompatibility and functionalization, focusing on their immunological interactions and synthesis methods to provide a comparative analysis and improve understanding of NDs' biomedical applications. Evaluation of *in vivo* biodistribution and dose-dependent toxicity is fundamental in researching this drug delivery system and offers key insights before introducing it to patients.

These findings reinforce that NDs demonstrate a favorable safety profile compared to other tested nanoparticles, thereby supporting their potential in biomedical applications. Moving forward, we will systematically examine how diverse surface modifications—encompassing chemical functionalization, polymeric coatings, and bioconjugation strategies—may influence ND biodistribution, cellular uptake, and immunogenicity (Yuan et al., 2009; Alexander and Leong, 2024). By delineating the design parameters that minimize toxicity while enhancing targeted delivery, we can refine ND-based platforms to maximize their therapeutic and imaging capabilities (Aillon et al., 2009a; Molaei, 2019). Moreover, recognizing the need for more comprehensive safety assessments, we will extend our investigations beyond acute exposures to include long-term studies evaluating chronic inflammation and immunomodulatory effects—crucial steps to ensure the successful clinical translation of ND-based nanoplatforms (Fischer and Chan, 2007; Blanco et al., 2015).

Ethical considerations in the *in vivo* use of nanoparticles demand rigorous safety assessments, transparent practices, and responsible innovation. Thorough toxicity, biodistribution, and chronic exposure studies must precede clinical applications to ensure a favorable risk-benefit balance. Compliance with regulatory standards (e.g., FDA, EMA) and oversight by ethics committees protects patient welfare, while clear communication of risks and benefits upholds informed consent. Ultimately, minimizing societal and environmental impacts and refining nanoparticle design are crucial for maintaining public trust.

In conclusion, our findings provide a deeper understanding of this evolving field of NPs and pave the way for further research. We recommend detailed studies that compare different exposure routes in multiple animal models and extend observation periods for longer durations.

Data availability statement

The original contributions presented in the study are included in the article/Supplementary Material, further inquiries can be directed to the corresponding author.

Ethics statement

The animal study was approved by the Association for Assessment and Accreditation of Laboratory Animal Care International (AAALAC). The study was conducted in accordance with the local legislation and institutional requirements.

Author contributions

EA: Conceptualization, Data curation, Formal Analysis, Supervision, Validation, Visualization, Writing – original draft, Writing – review and editing. KL: Writing – original draft, Writing – review and editing.

Funding

The author(s) declare that no financial support was received for the research and/or publication of this article.

Conflict of interest

The authors declare that the research was conducted in the absence of any commercial or financial relationships that could be construed as a potential conflict of interest.

Generative AI statement

The author(s) declare that no Generative AI was used in the creation of this manuscript.

Publisher's note

All claims expressed in this article are solely those of the authors and do not necessarily represent those of their affiliated organizations, or those of the publisher, the editors and the reviewers. Any product that may be evaluated in this article, or claim that may be made by its manufacturer, is not guaranteed or endorsed by the publisher.

Supplementary material

The Supplementary Material for this article can be found online at: https://www.frontiersin.org/articles/10.3389/fnano.2025.1512622/full#supplementary-material

References

Aillon, K. L., Xie, Y., El-Gendy, N., Berkland, C. J., and Forrest, M. L. (2009a). Effects of nanomaterial physicochemical properties on *in vivo* toxicity. *Adv. Drug Deliv. Rev.* 61 (6), 457–466. doi:10.1016/j.addr.2009.03.010

Aillon, K. L., Xie, Y., El-Gendy, N., Berkland, C. J., and Forrest, M. L. (2009b). Effects of nanomaterial physicochemical properties on *in vivo* toxicity. *Adv. drug Deliv. Rev.* 61 (6), 457–466. doi:10.1016/j.addr.2009.03.010

Albanese, A., Tang, P. S., and Chan, W. C. (2012). The effect of nanoparticle size, shape, and surface chemistry on biological systems. *Annu. Rev. Biomed. Eng.* 14, 1–16. doi:10.1146/annurev-bioeng-071811-150124

Alexander, A., Saraf, S., Saraf, S., Agrawal, M., Patel, R. J., Agrawal, P., et al. (2019). Amalgamation of stem cells with nanotechnology: a unique therapeutic approach. *Curr. Stem Cell. Res. Ther.* 14 (2), 83–92. doi:10.2174/1574888x13666180703143219

Alexander, E., and Leong, K. W. (2024). Immunomodulatory effects of laser-synthesized nanodiamonds on peripheral blood mononuclear cells: evaluation of unconjugated, PEGylated, and antibody-conjugated formulations. *Front. Nanotechnol.* 6. doi:10.3389/fnano.2024.1352287

Ansari, S. A., Satar, R., Jafri, M. A., Rasool, M., Ahmad, W., and Kashif Zaidi, S. (2016). Role of nanodiamonds in drug delivery and stem cell therapy. *Iran. J. Biotechnol.* 14 (3), 130–141. doi:10.15171/ijb.1320

Arvizo, R. R., Miranda, O. R., Moyano, D. F., Walden, C. A., Giri, K., Bhattacharya, R., et al. (2011). Modulating pharmacokinetics, tumor uptake and biodistribution by engineered nanoparticles. *PLoS One* 6 (9), e24374. doi:10.1371/journal.pone.0024374

Baidakova, M. V., Kukushkina, Y. A., Sitnikova, A. A., Yagovkina, M. A., Kirilenko, D. A., Sokolov, V. V., et al. (2013). Structure of nanodiamonds prepared by laser synthesis. *Phys. Solid State* 55 (8), 1747–1753. doi:10.1134/s1063783413080027

Bailly, A.-L., Correard, F., Popov, A., Tselikov, G., Chaspoul, F., Appay, R., et al. (2019). *In vivo* evaluation of safety, biodistribution and pharmacokinetics of laser-synthesized gold nanoparticles. *Sci. Rep.* 9 (1), 12890. doi:10.1038/s41598-019-48748-3

Blanco, E., Shen, H., and Ferrari, M. (2015). Principles of nanoparticle design for overcoming biological barriers to drug delivery. *Nat. Biotechnol.* 33 (9), 941–951. doi:10.1038/nbt.3330

Burgess, M., Gill, D., Singhania, R., Cheung, C., Chambers, L., Renyolds, B. A., et al. (2013). CD62L as a therapeutic target in chronic lymphocytic leukemia. *Clin. Cancer Res.* 19 (20), 5675–5685. doi:10.1158/1078-0432.ccr-13-1037

Caron, W. P., Song, G., Kumar, P., Rawal, S., and Zamboni, W. C. (2012). Interpatient pharmacokinetic and pharmacodynamic variability of carrier-mediated anticancer agents. *Clin. Pharmacol. Ther.* 91 (5), 802–812. doi:10.1038/clpt.2012.12

Cedervall, T., Lynch, I., Lindman, S., Berggård, T., Thulin, E., Nilsson, H., et al. (2007). Understanding the nanoparticle–protein corona using methods to quantify exchange rates and affinities of proteins for nanoparticles. *Proc. Natl. Acad. Sci.* 104 (7), 2050–2055. doi:10.1073/pnas.0608582104

Chang, S., Popowich, Y., Greco, R. S., and Haimovich, B. (2003). Neutrophil survival on biomaterials is determined by surface topography. *J. Vasc. Surg.* 37 (5), 1082–1090. doi:10.1067/mva.2003.160

Chew, A. K., Pedersen, J. A., and Van Lehn, R. C. (2022). Predicting the physicochemical properties and biological activities of monolayer-protected gold nanoparticles using simulation-derived descriptors. *ACS Nano* 16 (4), 6282–6292. doi:10.1021/acsnano.2c00301

Di Virgilio, F., Sarti, A. C., and Grassi, F. (2018). Modulation of innate and adaptive immunity by P2X ion channels. *Curr. Opin. Immunol.* 52, 51–59. doi:10.1016/j.coi.2018.03.026

Fischer, H. C., and Chan, W. C. (2007). Nanotoxicity: the growing need for *in vivo* study. *Curr. Opin. Biotechnol.* 18 (6), 565–571. doi:10.1016/j.copbio.2007.11.008

Ghoneum, M., Ghoneum, A., Tolentino, L., and Gimzewski, J. (2010). Modulation of aged murine T lymphocytes *in vivo* by DPV576-C, a nanodiamond- and nanoplatinum-coated material. *Vivo* 24 (2), 141–146.

Hammami, I., Alabdallah, N. M., jomaa, A. A., and kamoun, M. (2021). Gold nanoparticles: synthesis properties and applications. *J. King Saud Univ. - Sci.* 33 (7), 101560. doi:10.1016/j.jksus.2021.101560

Hare, J. I., Lammers, T., Ashford, M. B., Puri, S., Storm, G., and Barry, S. T. (2017). Challenges and strategies in anti-cancer nanomedicine development: an industry perspective. *Adv. Drug Deliv. Rev.* 108, 25–38. doi:10.1016/j.addr.2016.04.025

Harris, N. L., Watt, V., Ronchese, F., and Le Gros, G. (2002). Differential T cell function and fate in lymph node and nonlymphoid tissues. *J. Exp. Med.* 195 (3), 317–326. doi:10.1084/jem.20011558

Hauck, T. S., Anderson, R. E., Fischer, H. C., Newbigging, S., and Chan, W. C. W. (2010). *In vivo* quantum-dot toxicity assessment. *Small* 6 (1), 138–144. doi:10.1002/smll.200900626

Haziza, S., Mohan, N., Loe-Mie, Y., Lepagnol-Bestel, A. M., Massou, S., Adam, M. P., et al. (2017). Fluorescent nanodiamond tracking reveals intraneuronal transport abnormalities induced by brain-disease-related genetic risk factors. *Nat. Nanotechnol.* 12 (4), 322–328. doi:10.1038/nnano.2016.260

Huang, H., Pierstorff, E., Osawa, E., and Ho, D. (2007). Active nanodiamond hydrogels for chemotherapeutic delivery. *Nano Lett.* 7 (11), 3305–3314. doi:10.1021/nl071521o

Huang, K. J., Lee, C., Lin, Y., Lin, C., Perevedentseva, E., Hung, S., et al. (2017). Phagocytosis and immune response studies of Macrophage-Nanodiamond Interactions *in vitro* and *in vivo*. *J. Biophot.* 10 (10), 1315–1326. doi:10.1002/jbio.201600202

Iwamoto, T., Sugimoto, A., Kitamura, T., Akazawa, Y., and Hasegawa, T. (2014). The role of extracellular ATP-mediated purinergic signaling in bone, cartilage, and tooth tissue. *J. Oral Biosci.* 56 (4), 131–135. doi:10.1016/j.job.2014.07.003

Khan, H. A., Ibrahim, K. E., Alrashood, S. T., Alamery, S., Alrokayan, S. H., Al-Harbi, N., et al. (2020). Immunohistochemistry of IL-1β, IL-6 and TNF-α in spleens of mice treated with gold nanoparticles. *Saudi J. Biol. Sci.* 27 (4), 1163–1168. doi:10.1016/j.sjbs.2020.01.025

Kumar, M., Kulkarni, P., Liu, S., Chemuturi, N., and Shah, D. K. (2023). Nanoparticle biodistribution coefficients: a quantitative approach for understanding the tissue distribution of nanoparticles. *Adv. Drug Deliv. Rev.* 194, 114708. doi:10.1016/j.addr.2023.114708

Lazovic, J., Goering, E., Wild, A., Schützendübe, P., Shiva, A., Löffler, J., et al. (2024). Nanodiamond-enhanced magnetic resonance imaging. *Adv. Mater.* 36 (11), 2310109. doi:10.1002/adma.202310109

Lin, Y.-W., Su, H. C., Raj, E. N., Liu, K. K., Chang, C. J., Hsu, T. C., et al. (2023). Targeting EGFR and monitoring tumorigenesis of human lung cancer cells *in vitro* and *in vivo* using nanodiamond-conjugated specific EGFR antibody. *Pharmaceutics* 15 (1), 111. doi:10.3390/pharmaceutics15010111

Liu, C.-Y., Lee, M. C., Lin, H. F., Lin, Y. Y., Lai, W. Y., Chien, Y., et al. (2021). Nanodiamond-based microRNA delivery system promotes pluripotent stem cells toward myocardiogenic reprogramming. *J. Chin. Med. Assoc.* 84 (2), 177–182. doi:10.1097/jcma.0000000000000441

Liu, Z., Robinson, J. T., Sun, X., and Dai, H. (2008). PEGylated nanographene oxide for delivery of water-insoluble cancer drugs. *J. Am. Chem. Soc.* 130 (33), 10876–10877. doi:10.1021/ja803688x

Longmire, M., Choyke, P. L., and Kobayashi, H. (2008). Clearance properties of nano-sized particles and molecules as imaging agents: considerations and caveats. *Nanomedicine* 3 (5), 703–717. doi:10.2217/17435889.3.5.703

Lundqvist, M., Stigler, J., Elia, G., Lynch, I., Cedervall, T., and Dawson, K. A. (2008). Nanoparticle size and surface properties determine the protein corona with possible implications for biological impacts. *Proc. Natl. Acad. Sci. U. S. A.* 105 (38), 14265–14270. doi:10.1073/pnas.0805135105

Ma, Y., Gou, S., Zhu, Z., Sun, J., Shahbazi, M., Si, T., et al. (2024). Transient mild photothermia improves therapeutic performance of oral nanomedicines with enhanced

accumulation in the colitis mucosa. *Adv. Mater* 36 (14), e2309516. doi:10.1002/adma.202309516

McGuinness, L. P., Yan, Y., Stacey, A., Simpson, D. A., Hall, L. T., Maclaurin, D., et al. (2011). Quantum measurement and orientation tracking of fluorescent nanodiamonds inside living cells. *Nat. Nanotechnol.* 6 (6), 358–363. doi:10.1038/nnano.2011.64

Molaei, M. J. (2019). Carbon quantum dots and their biomedical and therapeutic applications: a review. *RSC Adv.* 9 (12), 6460–6481. doi:10.1039/c8ra08088g

Muller, J., Huaux, F., Moreau, N., Misson, P., Heilier, J. F., Delos, M., et al. (2005). Respiratory toxicity of multi-wall carbon nanotubes. *Toxicol. Appl. Pharmacol.* 207 (3), 221–231. doi:10.1016/j.taap.2005.01.008

Nair, A. B., and Jacob, S. (2016). A simple practice guide for dose conversion between animals and human. *J. Basic Clin. Pharm.* 7 (2), 27–31. doi:10.4103/0976-0105.177703

Nguyen, V. P., Qian, W., Zhe, J., Henry, J., Wang, M., Liu, B., et al. (2023). Renally clearable ultraminiature chain-like gold nanoparticle clusters for multimodal molecular imaging of choroidal neovascularization. *Adv. Mater* 35 (31), e2302069. doi:10.1002/adma.202302069

Paladhi, A., Rej, A., Sarkar, D., Singh, R., Bhattacharyya, S., Sarkar, P. K., et al. (2022). Nanoscale diamond-based formulation as an immunomodulator and potential therapeutic for lymphoma. *Front. Pharmacol.* 13, 852065. doi:10.3389/fphar.2022.852065

Patil, A. A., Descanzo, M. J. N., Agcaoili, J. B. A., Chiang, C. K., Cheng, C. L., Chang, H. C., et al. (2021). Carboxylated/oxidized diamond nanoparticles for quantifying immunoglobulin G antibodies using mass spectrometry. *ACS Appl. Nano Mater.* 4 (9), 8922–8936. doi:10.1021/acsanm.1c01553

Pentecost, A., Kim, M. J., Jeon, S., Ko, Y. J., Kwon, I. C., Gogotsi, Y., et al. (2019). Immunomodulatory nanodiamond aggregate-based platform for the treatment of rheumatoid arthritis. *Regen. Biomater.* 6 (3), 163–174. doi:10.1093/rb/rbz012

Perevedentseva, E., Peer, D., Uvarov, V., Zousman, B., and Levinson, O. (2015). Nanodiamonds of laser synthesis for biomedical applications. *J. Nanosci. Nanotechnol.* 15 (2), 1045–1052. doi:10.1166/jnn.2015.9747

Puzyr, A. P., Baron, A., Purtov, K., Bortnikov, E., Skobelev, N., Mogilnaya, O., et al. (2007). Nanodiamonds with novel properties: a biological study. *Diam. Relat. Mater.* 16 (12), 2124–2128. doi:10.1016/j.diamond.2007.07.025

Reagan-Shaw, S., Nihal, M., and Ahmad, N. (2008). Dose translation from animal to human studies revisited. *Faseb J.* 22 (3), 659–661. doi:10.1096/fj.07-9574lsf

Sangabathuni, S., Murthy, R. V., Chaudhary, P. M., Subramani, B., Toraskar, S., and Kikkeri, R. (2017). Mapping the glyco-gold nanoparticles of different shapes toxicity, biodistribution and sequestration in adult zebrafish. *Sci. Rep.* 7 (1), 4239. doi:10.1038/s41598-017-03350-3

Shao, D., Li, M., Wang, Z., Zheng, X., Lao, Y., Chang, Z., et al. (2018). Bioinspired diselenide-bridged mesoporous silica nanoparticles for dual-responsive protein delivery. *Adv. Mater* 30, e1801198. doi:10.1002/adma.201801198

Shulevitz, H. J., Amirshaghaghi, A., Ouellet, M., Brustoloni, C., Yang, S., Ng, J. J., et al. (2024). Nanodiamond emulsions for enhanced quantum sensing and click-chemistry conjugation. *ACS Appl. Nano Mater.* 7 (13), 15334–15343. doi:10.1021/acsanm.4c01699

Singh, D., and Ray, S. (2023). A short appraisal of nanodiamonds in drug delivery and targeting: recent advancements. *Front. Nanotechnol.* 5. doi:10.3389/fnano.2023.1259648

Song, G., Petschauer, J., Madden, A., and Zamboni, W. (2014). Nanoparticles and the mononuclear phagocyte system: pharmacokinetics and applications for inflammatory diseases. *Curr. Rheumatol. Rev.* 10 (1), 22–34. doi:10.2174/1573403x10666140914160554

Suarez-Kelly, L. P., Campbell, A. R., Rampersaud, I. V., Bumb, A., Wang, M. S., Butchar, J. P., et al. (2017). Fluorescent nanodiamonds engage innate immune effector cells: a potential vehicle for targeted anti-tumor immunotherapy. *Nanomedicine* 13 (3), 909–920. doi:10.1016/j.nano.2016.12.005

Suarez-Kelly, L. P., Sun, S. H., Ren, C., Rampersaud, I. V., Albertson, D., Duggan, M. C., et al. (2021). Antibody conjugation of fluorescent nanodiamonds for targeted innate immune cell activation. *ACS Appl. Nano Mater.* 4 (3), 3122–3139. doi:10.1021/acsanm.1c00256

Sun, Y. P., Fu, K., Lin, Y., and Huang, W. (2002). Functionalized carbon nanotubes: properties and applications. *Acc. Chem. Res.* 35 (12), 1096–1104. doi:10.1021/ar010160v

Tsai, L. W., Lin, Y. C., Perevedentseva, E., Lugovtsov, A., Priezzhev, A., and Cheng, C. L. (2016). Nanodiamonds for medical applications: interaction with blood *in vitro* and *in vivo*. *Int. J. Mol. Sci.* 17 (7), 1111. doi:10.3390/ijms17071111

van der Laan, K. J., Morita, A., Perona-Martinez, F. P., and Schirhagl, R. (2020). Evaluation of the oxidative stress response of aging yeast cells in response to internalization of fluorescent nanodiamond biosensors. *Nanomater. (Basel)* 10 (2), 372. doi:10.3390/nano10020372

Vega-Villa, K. R., Takemoto, J. K., Yáñez, J. A., Remsberg, C. M., Forrest, M. L., and Davies, N. M. (2008). Clinical toxicities of nanocarrier systems. *Adv. Drug Deliv. Rev.* 60 (8), 929–938. doi:10.1016/j.addr.2007.11.007

Villalba, P., Ram, M. K., Gomez, H., Bhethanabotla, V., Helms, M. N., Kumar, A., et al. (2012). Cellular and *in vitro* toxicity of nanodiamond-polyaniline composites in mammalian and bacterial cell. *Mater. Sci. Eng. C* 32 (3), 594–598. doi:10.1016/j.msec.2011.12.017

Williams, K. A., Veenhuizen, P. T. M., de la Torre, B. G., Eritja, R., and Dekker, C. (2002). Carbon nanotubes with DNA recognition. *Nature* 420 (6917), 761. doi:10.1038/420761a

Xing, Y., and Dai, L. (2009). *Nanodiamonds for nanomedicine. Nanomedicine (Lond)* 4 (2), 207–218. doi:10.2217/17435889.4.2.207

Xu, J.-Y., Li, Q. N., Li, J. G., Ran, T. C., Wu, S. W., Song, W. M., et al. (2007). Biodistribution of 99mTc-C60(OH)x in Sprague–Dawley rats after intratracheal instillation. *Carbon* 45 (9), 1865–1870. doi:10.1016/j.carbon.2007.04.030

Yang, L., Kuang, H., Zhang, W., Aguilar, Z. P., Wei, H., and Xu, H. (2017). Comparisons of the biodistribution and toxicological examinations after repeated intravenous administration of silver and gold nanoparticles in mice. *Sci. Rep.* 7 (1), 3303. doi:10.1038/s41598-017-03015-1

Yuan, Y., Chen, Y., Liu, J. H., Wang, H., and Liu, Y. (2009). Biodistribution and fate of nanodiamonds *in vivo*. *Diam. Relat. Mater.* 18 (1), 95–100. doi:10.1016/j.diamond.2008.10.031

Zappasodi, R., Budhu, S., Abu-Akeel, M., and Merghoub, T. (2020). *In vitro* assays for effector T cell functions and activity of immunomodulatory antibodies. *Methods Enzymol.* 631, 43–59. doi:10.1016/bs.mie.2019.08.012